Simulation and analysis of ^{13}N+p elastic resonance scattering*

WANG You-Bao(王友宝)[1)] QIN Xing(秦星) WANG Bao-Xiang(王宝祥) LIU Wei-Ping(柳卫平)
LI Zhi-Hong(李志宏) BAI Xi-Xiang(白希祥) LIAN Gang(连钢) GUO Bing(郭冰)
ZENG Sheng(曾晟) SU Jun(苏俊) LI Yun-Ju(李云居) JIANG Chao(蒋超)

(Department of Nuclear Physics, China Institute of Atomic Energy(CIAE), Beijing 102413, China)

Abstract The ^{13}N+p elastic resonance scattering has been studied at the secondary radioactive beam facility of CIAE in inverse kinematics via a thick-target method. The excitation function for the ^{13}N(p,p) scattering was obtained in the energy interval of $E_{\rm cm}\approx$0.5—3.2 MeV with a ^{13}N secondary beam of (47.8±1.5) MeV. Careful analysis of the secondary beam components and extensive Monte-Carlo simulations enable the resolution of the experimental proton spectra. The resonance parameters for five low-lying levels in ^{14}O were deduced by R-matrix fitting calculations with MULTI7 and SAMMY-M6-BETA. The present results show general agreement with those from a recent similar work, and thus confirm the observation of a new 0^- level at 5.7 MeV in ^{14}O with an improved width of 400(45) keV.

Key words radioactive secondary beam, elastic resonance scattering, excitation function, thick-target method

PACS 21.10.Hw, 25.40.Ny, 27.20.+n

1 Introduction

The advent of a radioactive nuclear beam provides exciting opportunities to explore the new frontiers in nuclear physics and nuclear astrophysics. To use a radioactive secondary beam of relatively low intensity and short half-life, unique experimental methods and techniques must be employed to meet the challenges not encountered in regular stable-beam experiments. Elastic resonance scattering in inverse kinematics with a thick-target is just one example[1, 2]. It uses either a solid[3—7] or a gas[8, 9] target containing hydrogen atoms, with a thickness flexible to map a single level or a range of excited states. The recoil protons give rise to the excitation function of an energy interval corresponding to the energy losses of the incident beam. The advantage of the method is that one can obtain the excitation function in a one-shot experiment with an acceptable accuracy. In Ref. [3], a low energy ^{7}Be beam of about 5 MeV was used to bombard a 270 μg/cm^2 thin $(CH_2)_n$ target, the excitation function of $E_{\rm cm}$ = 0.3—0.75 MeV was measured highlighting the 1^+ resonance at 0.77 MeV in ^{8}B. Relatively thicker $(CH_2)_n$ targets were used in several other experiments[4—6] that allowed for fully stopping the incident beams and the heavier reaction products; the measurements were therefore done with detectors at $\theta_{\rm lab} = 0^\circ$, which facilitated the physics analysis of the experimental excitation function. The method is also useful for stable beams; the 183 keV resonance in the ^{17}O(p,α)^{14}N reaction was recently measured by using an ^{17}O heavy-ion beam and a differentially-pumped windowless gas target[10].

Several secondary light-ion beams from ^{6}He to ^{18}F[11] are available at the radioactive secondary beam facility GIRAFFE[12] of the HI-13 Tandem accelerator laboratory. The ^{13}N secondary beam is among the ones with the best intensity. To extend our experimental research towards elastic resonance scattering, a proton ΔE-E counter telescope consisting of a 63 μm-thick Double-Sided Silicon Strip Detector(DSSSD) and a 982 μm-thick Multi-guard Silicon

Received 13 June 2008

* Supported by National Natural Science Foundation of China (10575136, 10735100) and Major State Basic Research Development Program (2007CB815003)

1) E-mail: ybwang@ciae.ac.cn

Quadrant(MSQ) detector was prepared and tested[13]. In thick-target resonant elastic scattering, since the energy of the ^{13}N ion decreases constantly along its trajectory, ^{14}O is formed at various low-lying excited states that promptly decay back into ^{13}N+p with the ^{13}N in its ground state. The ^{14}O states above the proton threshold can therefore be surveyed for the missing 0^- level and for the supplement of other resonance parameters[14]. Shortly before the present work, similar ^{13}N+p elastic resonance scattering was performed at the Center for Nuclear Study(CNS), Japan[6]. The main results of the present work have been reported elsewhere[15], therefore we place our emphasis on the simulation and data analysis of the ^{13}N+p scattering that were not gone into depth in the cited paper[15].

2 Experiment

The thick-target method demands clear knowledge of the secondary beam. For example, the accurate energy of the ^{13}N ions is useful for choosing a proper $(CH_2)_n$ target thickness. Besides, one needs to know the contaminants in the secondary beam to design the detector geometry to avoid direct bombardment by leaked components.

2.1 ^{13}N secondary beam

The ^{2}H(^{12}C,^{13}N)n reaction was used to produce the ^{13}N ions with a ^{12}C beam of 72 MeV and intensity of about 100—150 pnA. After magnetic separation and focus, the secondary beam was further purified by a Wien velocity filter, and was collimated by a ϕ9—ϕ5 mm collimator complex. Choosing such a collimator complex with the diameters larger than used before is for the ^{13}N intensity. During the experiment, the intensity of the secondary beam was about 6000—10000 particles/s, and the purity about 82%—90%. A ΔE-E_t scatter plot of the ^{13}N secondary beam is shown in Fig. 1.

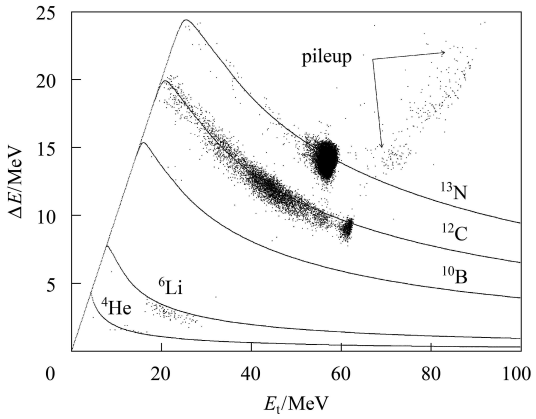

Fig. 1. The scatter plot of ΔE-E_t of the ^{13}N secondary beam, which was taken by a set of beam-tuning silicon ΔE-E telescopes 19 and 300 μm in thickness, respectively. The calculated energy loss of each kind of nuclide is presented in solid lines.

The ^{6}Li and ^{4}He contaminants were due to the ^{2}H(^{12}C,^{6}Li)^{8}Be and ^{2}H(^{12}C,α)^{10}B reactions, respectively. These light components if leaked will deposit in the DSSSD, and therefore spoil the proton spectrum below 2.5 MeV (the stopping power of the DSSSD for protons). Due to their small amounts, a detector ahead of the $(CH_2)_n$ target can resolve this. The higher-energy group of ^{12}C contaminants is a hazardousness for the $\theta_{lab} = 0°$ detector geometry, when penetrating the target with a thickness suitable for the ^{13}N, it can cause serious malfunction of the DSSSD.

2.2 Experimental setup

A schematic layout of the experimental setup for the ^{1}H(^{13}N,p)^{13}N reaction is shown in Fig. 2. To avoid the direct bombardment of the DSSSD by the leaked ^{12}C and light ion contaminants, the proton ΔE-E telescope was placed at 15° instead of 0°.

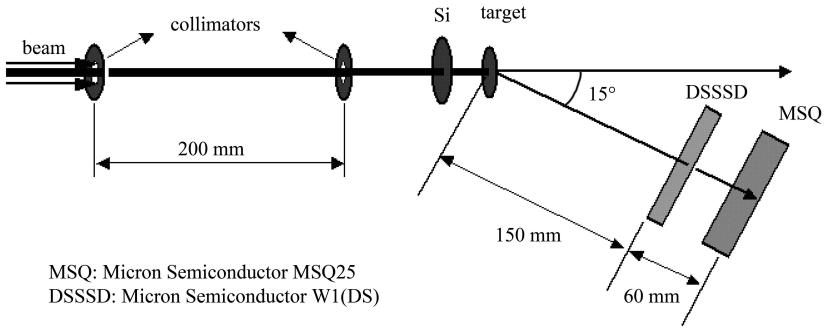

Fig. 2. Schematic layout of the experimental setup.

A 13.2 μm thin ORTEC silicon detector was used to monitor the secondary beam in front of the 9.33 mg/cm^2 $(CH_2)_n$ target. The role of the detector was to record the beam for normalization, and to remove proton events generated from ions other than ^{13}N. The energy of the ^{13}N ions impinging on the $(CH_2)_n$ target was about (47.8±1.5) MeV; a carbon foil of 10.88 mg/cm^2 in thickness was employed to evaluate the background arising from the carbon atoms in the $(CH_2)_n$ target. The silicon detector substituted the time-of-flight setup introduced in our previous work[16], because significant beam losses were found due to the generated angular divergence when secondary ions passed the scintillator foil of the front timing detector.

The experimental proton spectrum was calibrated with proton beams scattering on Au of 440 μg/cm^2 at several energies, and with a standard ^{239}Pu-^{241}Am mixed source. Due to the limitation of the available data acquisition system, only half of the DSSSD area was used while the outer part was blocked. For the inner half thus used, the DSSSD covered about 10°—20° in the laboratory frame, corresponding to 140°—160° in the center of the mass frame.

3 Simulation and data analysis

The complexity in the analysis of a thick-target experimental data lies in the fact that at any individual angle, the proton energy spectrum is continuous over a certain range. Therefore, the reaction kinematics must be rebuilt taking into account the energy losses of particles in the target for each detector cell within the experimental angular resolution. Monte-Carlo simulation combining the reaction kinematics with the energy straggling of ions in the target has been employed for this purpose.

3.1 Experimental E_{cm} resolution

To convert the detected proton total energies into E_{cm}, one needs to know the energy losses of the protons in the $(CH_2)_n$ target according to each θ_{lab}. This was done with a Monte-Carlo simulation combining the reaction kinematics with the energy losses of ^{13}N and protons. In the simulation, the θ_{lab} resolution was taken as 2.5°(FWHM), mainly resulting from the beam angular resolution(1.4°) and the beam spot(1.9°). As an example, the proton energy loss in the $(CH_2)_n$ target versus the detected proton total energy at $\theta_{lab} = 12.7°$ is shown in Fig. 3.

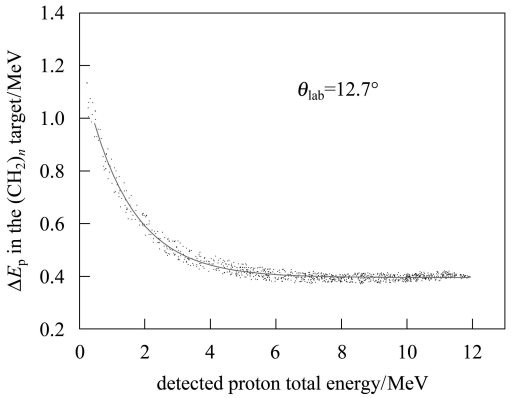

Fig. 3. The simulated proton energy loss in the $(CH_2)_n$ target versus the detected proton total energy for a pixel centered at $\theta_{lab} = 12.7°$. Each pixel of the DSSSD was thus simulated and fitted with a first order exponential decay function to retrieve the proton energy loss in the target.

Combining the proton energy loss in the $(CH_2)_n$ target with the detected total energy, the proton energy E_p at the reaction point was obtained, which was then converted into E_{cm} by the following formula.

$$E_{cm} = E_p \times \frac{m_1 + m_{13}}{4m_{13}\cos^2\theta_{lab}} , \quad (1)$$

where m_1 and m_{13} are the masses of the proton and ^{13}N, respectively, and θ_{lab} is the scattering angle. In the course of E_p to E_{cm} conversion, the uncertainty of E_{cm} was estimated to be ± 20 keV mainly due to the θ_{lab} resolution and the energy straggling of particles in the target as shown in Fig. 4.

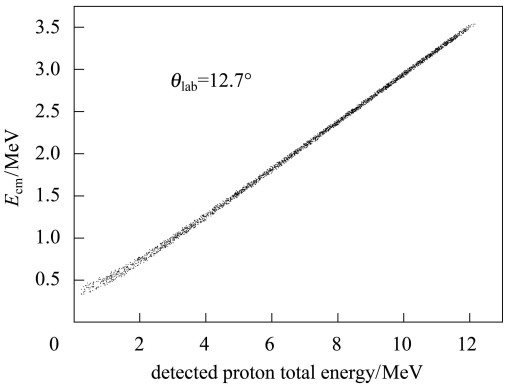

Fig. 4. The simulated E_{cm} versus the detected proton total energy for a pixel centered at $\theta_{lab} = 12.7°$. The lower threshold is about 500 keV in E_{cm} with a resolution of about ±20 keV.

3.2 Experimental proton yield

After the E_p to E_{cm} conversion, the proton yields were added up over different θ_{lab}. The higher-energy part of the summed experimental proton yield is shown in Fig. 5 together with that from the carbon

target. One can see from Fig. 5 that the proton yield from the $(CH_2)_n$ target has a clear structure while the one from the carbon target is rather flat. In the analysis of the calibrated data, these proton events were selected with the DSSSD-MSQ particle identification and the coincidence with the ^{13}N recorded in the 13.2 μm ΔE. For the protons below 2.5 MeV that were stopped in the DSSSD, the same coincidence criterion was applied also requesting the MSQ as a veto. In this way, the low-energy protons from the ^{1}H(^{13}N,p)^{13}N reaction were fortunately discernible.

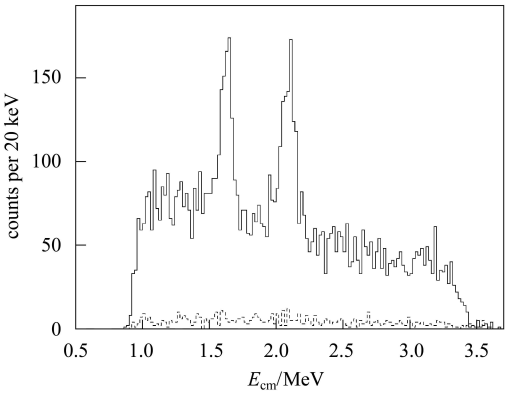

Fig. 5. Part of the summed experimental proton yield.

3.3 Background subtraction

The proton yields with the carbon target were normalized to those with the $(CH_2)_n$, by the total number of the ^{13}N ions and by the number of carbon atoms in the effective target thickness related to per E_{cm} unit. The latter was done by computing the range difference, i.e., the ^{13}N range difference between the maximum and the minimum energies of per E_{cm} unit in the $(CH_2)_n$ and carbon, respectively. The net proton yields were then obtained by subtracting the normalized background events of the carbon target.

3.4 Differential cross section

The net proton yields of ^{13}N+p were converted into the averaged differential cross section according to

$$\frac{\mathrm{d}N_\mathrm{p}}{\mathrm{d}E} = N_{^{13}\mathrm{N}} \frac{\mathrm{d}N_\mathrm{target}}{\mathrm{d}E} \left(\frac{\mathrm{d}\sigma}{\mathrm{d}\Omega}\right)_\mathrm{lab} \mathrm{d}\Omega \ . \tag{2}$$

In the formula, $\mathrm{d}N_\mathrm{p}/\mathrm{d}E$ refers to the net proton yield of per E_{cm} unit, $\mathrm{d}N_\mathrm{target}/\mathrm{d}E$ the energy dependent hydrogen atom number. As mentioned before, the effective target thickness was computed by the ^{13}N range difference between the maximum and the minimum energies of per E_{cm} unit in the $(CH_2)_n$. In addition, it was also checked by the Monte-Carlo simulation of the target depth versus E_{cm} where the scattering took place, as shown in Fig. 6. The divergence of the two methods is less than 1%.

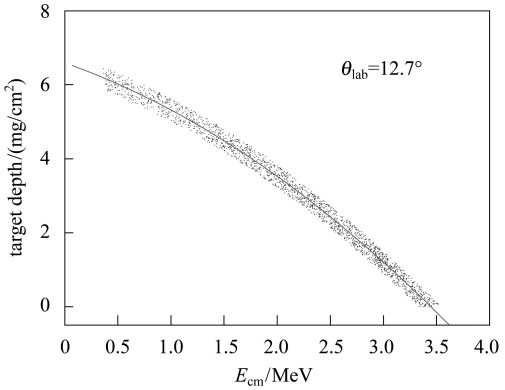

Fig. 6. The simulated target depth vs E_{cm} where the scattering takes place. The data were fitted by a two-order polynomial function to obtain a relation that is angle independent. The effective target thickness of per E_{cm} unit is then the corresponding depth difference in the vertical axis.

Taking account of $\theta_{cm} = 180° - 2\theta_{lab}$, the averaged $\mathrm{d}\sigma/\mathrm{d}\Omega$ in the center of the mass frame was obtained simply by

$$\left(\frac{\mathrm{d}\sigma}{\mathrm{d}\Omega}\right)_\mathrm{cm} = \frac{1}{4\cos\theta_\mathrm{lab}} \left(\frac{\mathrm{d}\sigma}{\mathrm{d}\Omega}\right)_\mathrm{lab} . \tag{3}$$

3.5 Absolute errors

Although the absolute value of the differential cross section is not a necessity in the deduction of the resonance parameters, it is obtainable by taking account of the contributing errors. Besides the statistical error of the net proton yield, systematical uncertainties were estimated on the remaining items in Eq. (2) including the uncertainties of the detector solid angle (4%), of beam normalization caused by the pile-up reject and the coincidence criterion (6%), and of the hydrogen atom number (4%) (see Fig. 6). The total systematical uncertainty that contributes to the differential cross section is roughly 8%.

4 *R*-matrix analysis and results

4.1 *R*-matrix background

The general formalism to describe the resonant process in a low-energy nuclear reaction is R-matrix theory[17]. The theory makes use of the compound nucleus hypothesis, which separates a two-body nuclear reaction process into two independent steps: the formation and the decay of an intermediate compound

nucleus. For every reaction (decay) channel, a channel radius a_c is defined and the resonance can take place only in the internal region. A commonly used prescription for the channel radius is

$$a_c = r_0(A_1^{1/3} + A_2^{1/3}) \ , \tag{4}$$

where A_1 and A_2 are the masses in μ of the ejectile and residue, respectively. r_0 is called the unit radius, which is independent of A_1 and A_2 and has a numerical value between 1.40 and 1.50 fm.

The reaction cross globule section $\sigma^J_{cc'}$ is conventionally written in terms of the collision matrix $U^J_{cc'}$ from the incoming channel c to the outgoing channel c′.

$$\sigma_{cc'} = \frac{\pi}{k_c^2}\sum_J \frac{2J+1}{(2I_1+1)(2I_2+1)} \times \left|\exp(2i\omega_c)\delta_{cc'} - U^J_{cc'}\right|^2 \ , \tag{5}$$

where k_c is the wave number, and ω_c is the Coulomb phase shift. The R-matrix theory relates the collision matrix with a complete set of the internal functions via the R-matrix by boundary conditions. The R-matrix $R_{c'c}$ is defined as

$$R_{c'c} = \sum_\lambda \frac{\gamma_{\lambda c}\gamma_{\lambda c'}}{E_\lambda - E} \ , \tag{6}$$

where λ denotes the level index. The reduced widths $\gamma^2_{\lambda c}$ are related with the Coulomb penetrability $P(l)$ by

$$\gamma^2_{\lambda c} = \Gamma_{\lambda c}/2P(l) \ , \tag{7}$$

and the $P(l)$ are defined by

$$P(l) = kr/(F_l^2 + G_l^2)\,|_{a_c} \ , \tag{8}$$

where F_l and G_l are the regular and irregular Coulomb functions, respectively. In the case of proton elastic resonance scattering, the differential cross section can be written into a sum of pure Coulomb, resonant (reaction), and interference terms.

4.2 Elastic resonance channels

The ground state of ^{13}N has a spin and parity of $1/2^-$, which is probably of the proton $1p_{1/2}$ state. The channel spin of ^{13}N+p has two values, $s_c = 1^-$ or 0^-, therefore a s-wave proton resonance ($2s_{1/2}$) directly populates the 1^- and 0^- states in ^{14}O. For the E_{cm} range in this work, $P(l)$ decrease rapidly as l increase, the reduced widths for $l+2$ normally exceed the single-particle Wigner limit of $\gamma^2 \leqslant \hbar^2/\mu a_c^2$, and $l+2$ mixing is therefore neglected. The elastic resonance channels for the decay of ^{14}O$^* \rightarrow ^{13}$N$_{gs}$+p are listed in Table 1. Channel spin mixing can occur for 1^+ and 2^- states in ^{14}O, which correspond to the mixings of the proton $p_{1/2}$ and $p_{3/2}$, $d_{3/2}$ and $d_{5/2}$ orbitals, respectively.

Table 1. The allowed elastic resonance channels for the decay of ^{14}O$^*\rightarrow^{13}$N$_{g.s.}$+p.

I^π	s_c	l	j_p
0^-	0^-	0	$2s_{1/2}$
0^+	1^-	1	$1p_{1/2}$
1^-	1^-	0	$2s_{1/2}$
1^+	0^-, 1^-	1	$1p_{1/2}$, $1p_{3/2}$
2^-	0^-, 1^-	2	$1d_{3/2}$, $1d_{5/2}$
2^+	1^-	1	$1p_{3/2}$
3^-	1^-	2	$1d_{5/2}$

4.3 Results and discussion

The experimental excitation function for ^{13}N+p scattering is shown in Fig. 7. The fitting calculation was performed by using the multilevel R-matrix codes MULTI7[18] and SAMMY-M6-BETA. The input parameters include the resonance energy, width, spin and parity, while s_c and l are subject to the conservation laws. With MULTI7, one can calculate the differential cross section taking into account the channel spin mixing and orbital angular momentum mixing. The theoretical differential cross section can be normalized to the experimental one by comparing the area under the curve. SAMMY-M6-BETA enables multilevel R-matrix fits to the experimental excitation function by solving the Bayes equations. In the analysis, MULTI7 was used first to obtain a 'best' set of the resonance parameter, which was then finely tuned by SAMMY-M6-BETA to yield the final values and uncertainties as well.

The experimental excitation function covers the energy interval of $E_{cm} \approx$0.5—3.2 MeV, in which five low-lying proton resonance states in ^{14}O are discernible. In general, the odd-parity low-spin states are more favorable to populate by the ^{13}N+p entrance channel with $l = 0, 2$, while the population of 0^+ and 2^+ levels with $l = 1$ partial waves is suppressed at large θ_{cm} angles. The deduced width for the astrophysical important 1^- level (40 ± 4) keV agrees well with the latest adopted value of (37.3±0.9) keV[19, 20]. For the s-wave 0^- new level at 5.7 MeV, the present work exhibits its domain more clearly than that in Ref. [6], which helps to determine a more accurate width of 400(45) keV. The d-wave 3^- state at 6.3 MeV is a puzzle as far as its width is concerned. The earlier compilation[14] suggested a value of (103±6) keV, which was not justified by the results of (50 ± 6) keV and (42 ± 2) keV from a study of charge exchange reaction ^{14}N(^{3}He,t)^{14}O[21] and very recent ^{13}N+p resonance scattering[6], respectively. To fit the amplitude

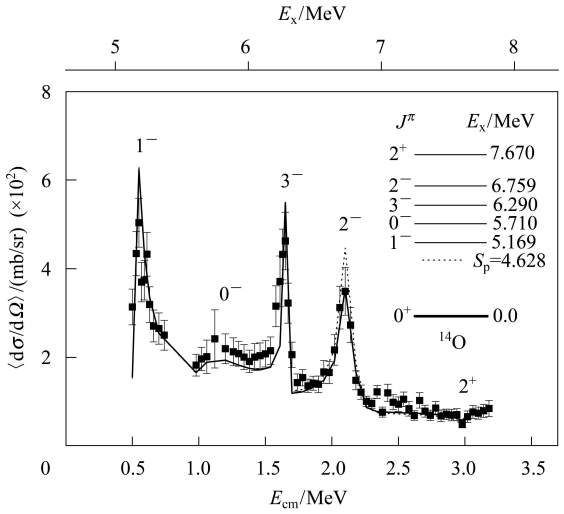

Fig. 7. The experimental excitation function for ^{13}N+p scattering. The gaps at E_{cm} = 0.8 MeV are due to the detector dead layers. The insert shows the observed ^{14}O levels in the experiment. The best fitting result is indicated by the solid line. The dotted line represents a fitting calculation with only $s_c = 0$ for the 2^- state.

of the experimental peak, an even smaller value of (25 ± 3) keV was found to be suitable in the present work. The channel spin mixing was checked for the 2^- level at 6.8 MeV in ^{14}O. The experimental excitation function can be fitted equally well with pure $s_c = 1$ (solid line in Fig. 7) or with mixing up to 1:1. The pure $s_c = 0$ (dotted line in Fig. 7) does not fit the peak amplitude.

5 Summary

In summary, the thick-target method has been successfully applied for the study of ^{13}N+p elastic resonance scattering. The excitation function was obtained over a wide energy range with a single bombarding energy of the ^{13}N secondary beam. Careful analysis of the secondary beam components and extensive Monte-Carlo simulations enable the resolution of the experimental proton spectra. The resonance parameters for five low-lying levels in ^{14}O were deduced by R-matrix fitting calculations of the experimental excitation function. The present results show general agreement with those from a recent similar work, thus confirming the observation of a new 0^- level at 5.7 MeV in ^{14}O with an improved width of 400(45) keV. However, the remarkable discrepancy of the proton width for the 3^- level at 6.3 MeV deserves a more detailed investigation, preferably with an intensive ^{13}N beam and at more angles.

The authors thank Professor John Shriner of Tennessee Technological University for providing the R-matrix code MULTI7. We also wish to thank the technical staff of the HI-13 Tandem laboratory for preparing the targets and carefully operating the machine.

References

1 Kubono S. Nucl. Phys. A, 2001, **693**: 221
2 Smith M S, Rehm K E. Annu. Rev. Nucl. Part. Sci., 2001, **51**: 91
3 Angulo C, Azzouz M, Descouvemont P et al. Nucl. Phys. A, 2003, **716**: 211
4 Teranishi T, Kubono S, Shimoura S et al. Phys. Lett. B, 2003, **556**: 27
5 Gómez del Campo J, Galindo-Uribarri A, Beene J R et al. Phys. Rev. Lett., 2001, **86**: 43
6 Teranishi T, Kubono S, Yamaguchi H et al. Phys. Lett. B, 2007, **650**: 129
7 Ruiz C, Davinson T, Sarazin F et al. Phys. Rev. C, 2005, **71**: 025802
8 Axelsson L, Borge M J G, Fayans S et al. Phys. Rev. C, 1996, **54**: R1511
9 Markenroth K, Axelsson L, Baxter S et al. Phys. Rev. C, 2000, **62**: 034308
10 Moazen B H, Bardayan D W, Blackmon J C et al. Phys. Rev. C, 2007, **75**: 065801
11 LI Zhi-Hong, LIU Wei-Ping, BAI Xi-Xiang et al. HEP & NP, 2006, **30**(Suppl. Ⅱ): 258 (in Chinese)
12 BAI Xi-Xiang, LIU Wei-Ping, QIN Jiu-Chang et al. Nucl. Phys. A, 1995, **588**: 273c
13 WANG You-Bao, WANG Bao-Xiang, BAI Xi-Xiang et al. HEP & NP, 2006, **30**(Suppl. Ⅱ): 202 (in Chinese)
14 Ajzenberg-Selove F. Nucl. Phys. A, 1991, **523**: 1
15 WANG You-Bao, WANG Bao-Xiang, QIN Xing et al. Phys. Rev. C, 2008, **77**: 044304
16 QIN Xing, WANG You-Bao, WANG Bao-Xiang et al. Atomic Energy Science and Technology, 2008, **42**: 452 (in Chinese)
17 Lane A M, Thomas R G. Rev. Mod. Phys., 1958, **30**: 257
18 Nelson R O, Bilpuch E G, Mitchell G E. Nucl. Instrum. Methods Phys. Res. A, 1985, **236**: 128
19 TANG Xiao-Dong, Azhari A, FU Chang-Bo et al. Phys. Rev. C, 2004, **69**: 055807
20 LI Zhi-Hong, GUO Bing, YAN Sheng-Quan et al. Phys. Rev. C, 2006, **74**: 035801
21 Negret A, Adachi T, Berg G P A et al. Phys. Rev. C, 2005, **71**: 047303